Journal of Materials Chemistry A

PAPER

View Article Online
View Journal | View Issue

Cite this: J. Mater. Chem. A, 2016, 4, 2263

Unprecedented performance of N-doped activated hydrothermal carbon towards C_2H_6/CH_4, CO_2/CH_4, and CO_2/H_2 separation†

Bin Yuan,‡ Jun Wang,§ Yingxi Chen,‡ Xiaofei Wu,¶ Hongmei Luo and Shuguang Deng§*

Received 20th October 2015
Accepted 8th January 2016

DOI: 10.1039/c5ta08436a

www.rsc.org/MaterialsA

A series of N-doped porous carbons with different textural properties and N contents was prepared from a mixture of algae and glucose and their capability for the separation of CO_2/CH_4, C_2H_6/CH_4, and CO_2/H_2 binary mixtures under different conditions (bulk pressure, mixture composition, and temperature) were subsequently assessed in great detail. It was observed that the gas (C_2H_6, CO_2, CH_4, and H_2) adsorption capacity at different pressure regions was primarily governed by different adsorbent parameters (N level, narrow micropore volume, and BET specific surface area). More interestingly, it was found that N-doping can selectively enhance the heats of adsorption of C_2H_6 and CO_2, while it had a negligible effect on those of CH_4 and H_2. The adsorption equilibrium selectivities for separating C_2H_6/CH_4, CO_2/CH_4, and CO_2/H_2 gas mixture pairs on the porous carbons were predicted using the ideal adsorbed solution theory (IAST) based on pure-component adsorption isotherms. In particular, sample NAHA-1 exhibited by far the best performance (in terms of gas adsorption capacity and selectivity) reported for porous carbons for the separation of these three binary mixtures. More significantly, NAHA-1 carbon outperforms many of its counterparts (*e.g.* MOFs and zeolites), emphasizing the important role of carbonaceous adsorbents in gas purification and separation.

1 Introduction

The ever-increasing accumulation of greenhouse gases (GHG) (*e.g.* CO_2 and CH_4) in the atmosphere is significantly responsible for the severely detrimental global warming and concomitant climate changes and other environmental issues, which is a worldwide concern and has attracted considerable attention. In order to mitigate the impact of the greenhouse effect on the environment, the amount of greenhouse gas emission into the atmosphere should be capped. In this regard, there are currently two major strategies under extensive investigations. One is by large-scale greenhouse gas capture for carbon neutrality[1–4] in view of the fact that fossil fuel based energy economy will continue to predominate for, at least, the next few decades. The other is by using alternative cleaner energy carriers that produce a lower amount amount of greenhouse gases per energy unit to achieve a low-carbon-based (or even non-carbon based) economy.[5–8]

With respect to greenhouse gas capture, most of the attention has been placed on post-combustion CO_2 capture from main stationary anthropogenic point sources, such as fossil fuel (*e.g.* coal) fired power plants possibly because (i) CO_2 is the major contributor to global warming among all the greenhouse gases due to its considerable emission quantity,[9] although it has the smallest global warming potential (GWP),[10] and (ii) it is viable to retrofit the technology of post-combustion CO_2 capture to conventional power plants.[11] However, more attention needs to be paid to pre-combustion CO_2 capture (*i.e.* capturing CO_2 from H_2) or CH_4 capture and utilization as (i) pre-combustion CO_2 capture is more cost-effective and provides a clean energy carrier, *i.e.* H_2,[12,13] (ii) CH_4 accounts for about 14% of the global GHG emission and has tremendously higher GWP than CO_2.[9,14] The emission sources of CH_4 include, but are not limited to, the spots that emit landfill gas, biogas, shale gas, and coal seam gas. Methane in these gases is generally mixed with CO_2, C_2H_6, and other kinds of trace components. Therefore, pre-combustion CO_2 capture and CH_4 capture and utilization for environmental protection typically involve the separation of CO_2/CH_4, C_2H_6/CH_4, and CO_2/H_2 gas mixture pairs.[9,14,15]

Department of Chemical & Materials Engineering, New Mexico State University, Las Cruces, NM 88003, USA. E-mail: shuguang.deng@asu.edu; Fax: +1-480-727-9321; Tel: +1-480-727-7238

† Electronic supplementary information (ESI) available. See DOI: 10.1039/c5ta08436a

‡ Present address: Department of Chemical & Biological Engineering, Iowa State University of Science and Technology, Sweeney Hall, Ames, IA 50011, USA.

§ Present address: School for Engineering of Matter, Transport, and Energy, Arizona State University, 551 E. Tyler Mall, Tempe, AZ 85287, USA.

¶ Present address: Ningbo Institute of Materials Technology & Engineering, Chinese Academy of Science, 1219 Zhongong West Road, Ningbo, Zhejiang Province, 315201, China.

In the case of using cleaner energy carriers, natural gas and hydrogen as promising alternatives to gasoline have attracted great interest. Methane, the primary component of natural gas, generates the smallest quantity of CO_2 per unit of energy release amongst all forms of fossil fuels (*e.g.* coal and petroleum) and hydrocarbons owing to its highest hydrogen to carbon ratio.[16,17] Along with its other features, such as natural abundance and ready availability, natural gas is widely accepted as a fuel to bridge the gap between oil-and-coal-based fuels and environmentally friendly, sustainable fuels. Hydrogen is considered as an absolutely clean and environmentally benign energy carrier due to its zero-emission combustion.[18] Another fascinating character of hydrogen, among many others, is its highest energy density by mass. These advantages, thereby, make natural gas and hydrogen as attractive candidates of fuel that can help govern the GHG concentration in the atmosphere.

Production of natural gas and hydrogen that meet the demanding requirements for efficient practical applications is the crucial first step towards their ubiquity and predominance. The amount of CO_2, one of the most common contaminants of natural gas, should be reduced to a certain level prior to the utilization of natural gas as it (i) lowers the conversion rate and heating value of natural gas, (ii) leads to corrosion of pipelines and equipment, and (iii) reduces the throughput of the pipeline for methane.[19,20] Indeed, removal of CO_2 from natural gas is incorporated into the industrial natural gas sweetening process.[4] Besides CO_2, light hydrocarbons, for example, ethane (C_2H_6), are another kind of major impurity and should be separated from natural gas as well since they are very popular chemical feedstocks and energy resources in a wide range of industrial processes.[21–23] A substantial amount of hydrogen can be generated from renewable biomass through chiefly three sequential steps: syngas formation by steam reforming, water-gas shift reaction, and CO_2 removal.[6,24–27] Consequently, the production of high purity natural gas and hydrogen also demands the separation of the gas mixtures of CO_2/CH_4, C_2H_6/CH_4, and CO_2/H_2.

To date, a multitude of approaches have been explored for gas separation and purification. Chemical absorption and cryogenic distillation are two of the most important ones and widely used in industry partially due to their superior selectivity. However, the parasitic energy penalty associated with these two techniques is surprisingly high.[28–31] Taking the amine-scrubbing technique for the removal CO_2 from flue gas as an example of chemical absorption, the regeneration of the aqueous alkanolamine solution is so energy-costly that it can take up more than 20% of the output energy of a power plant.[32] Physical adsorption, such as pressure, temperature, and vacuum swing adsorption, by porous solid materials is currently regarded as the most promising method and has attracted intense research interest for at least two reasons: high energy efficiency and ease of operation.[30,31] The moderate reversible physisorption gives rise to easy cost-effective regeneration and in turn the overall low energy cost of operation. One prerequisite to make the physisorption-based separation economically more competitive in practical application is a powerful and robust adsorbent. Two vital criteria that have been most broadly used to assess the performance of an adsorbent are: selectivity and adsorption capacity.[33,34]

To this day, immense effort has been devoted to developing suitable adsorbents for selective gas capture. Of the diverse porous adsorbents, metal organic frameworks (MOFs), zeolites, and carbon-based materials are very fascinating in clean energy and environmental applications and have been extensively investigated due to their large surface area and pore volume, and tunable pore size, all of which greatly underlie their adsorptive performance. UTSA-16 (MOF) has been recently reported to have an exceptional CO_2 uptake of 160 cm^3 cm^{-3} at 296 K and 1 bar and ultrahigh CO_2/CH_4 selectivity.[35] Farha and co-workers reported that NU-100 (MOF) exhibits a remarkable total CO_2 adsorption capacity of 2315 mg g^{-1} at 298 K and 40 bar.[36] The pore size of the partially Sr exchanged ETS-4 (zeolite) can be finely manipulated by the dehydration temperature and the resulting frameworks showed great potential for separating the CH_4/C_2H_6 mixture.[37] It is reported that zeolite SSZ-13 can display a superior CH_4/N_2 selectivity of over 70.[38] Single-walled carbon nanotubes have been studied for hydrogen storage.[39]

Besides the aforementioned screening criteria for the adsorptive and separation performance, other factors that are related to an adsorbent, such as the simplicity of synthesis, density, scalability, sustainability, availability, physicochemical stability, cost, hydrophobicity, and toxicity, are of great significance as well. Herein, we would like to assign a term, "inherent criteria", to these factors, in contrast to the performance criteria. Although remarkable progress has been achieved on the development of adsorbents, few materials, unfortunately, can satisfactorily meet both the performance criteria and the inherent criteria. For instance, most of the reported MOFs suffer from chemical and hydrothermal instabilities, high cost, and complicated, small-scale, and toxic synthesis.[40] The two key drawbacks of zeolites, *i.e.* low regenerability and intense hydrophilic nature, severely constrain their potential in industrial applications.[17,41] Hence, at this early stage, there remains a plethora of challenges in developing diverse materials that can easily satisfy the stringent standards. Carbon-based materials are extremely promising,[42] especially in meeting the inherent criteria.

Hydrothermal carbonization has recently experienced a renaissance serving as the most sustainable synthetic pathway for the production of carbonaceous materials from renewable and sustainable biomass, an inexpensive, highly abundant, easily accessible, nontoxic carbon feedstock.[43] Compared with the conventional pyrolysis process, hydrothermal carbonization exhibits mainly the following crucial advantages: (i) employing a relatively mild synthesis temperature (generally 423–623 K), (ii) being applicable to wet feedstocks with high water content and avoiding costly drying processes; (iii) showing higher carbon yield;[44] (iv) generating a much lower amount of greenhouse gases; (v) being energy-efficient as hydrothermal carbonization is an exothermic process; (vi) lowering the mineral content in the hydrothermal carbon (HTC).[45] Moreover, hydrothermal carbonization can help reduce the landfill gas emission by making use of waste biomass and offers an efficient approach for carbon sequestration on a large scale.[46–48]

So far, surprisingly very limited efforts have been made to investigate the potential applications of hydrothermal carbon and its derivatives in greenhouse gas capture and clean energy purification,[49–52] although they have already shown great potential.[53–55] For instance, M. Sevilla *et al.* have demonstrated that activated carbon derived from hydrothermally treated cellulose is a promising adsorbent for H_2 storage with a H_2 storage density up to 16.4 μmol H_2 per m^2.[49] Activated hydrothermal carbon from sawdust exhibited a high CO_2 uptake capacity of 4.8 mmol g^{-1} at 1 bar and 298 K.[51] To the best of the author's knowledge, there has been only one report on separation of CO_2/CH_4 very recently using activated hydrothermal carbon that is made from pure carbohydrates (sucrose) instead of biomass.[14] And no information on the C_2H_6/CH_4 or CO_2/H_2 separation from HTC or its derivatives has been reported yet. It is urgently demanded to evaluate the capability of biomass-involved HTC and its derivatives in clean energy (CH_4 and H_2) upgrading and GHG (CO_2, CH_4) capture.

In this study, nitrogen-doped porous carbons from a mixture of algae and glucose were synthesized in view of the following facts: (i) carbonaceous adsorbents generally have relatively low adsorption capacity and selectivity, (ii) N-doping is an effective strategy to significantly improve the gas adsorption and separation performance of adsorbents, (iii) N-doped hydrothermal carbon can be readily achieved by using suitable nitrogen-containing biomass, and (iv) algae has many attractive advantages (*e.g.* high growth rate and high productivity). They were employed for the first time as an example of carbonaceous adsorbents derived from biomass-involved (as opposed to pure carbohydrate-based) HTC to thoroughly demonstrate their outstanding performance regarding the separation of CO_2/CH_4, C_2H_6/CH_4, and CO_2/H_2 binary mixtures.

2 Experimental section

2.1 Synthesis of activated hydrothermal carbon

N-doped activated hydrothermal carbons from a mixture containing algae and glucose (denoted as NAHA) were prepared by referring to the previously reported procedures.[52,56] Briefly, 13.5 g of dry *Nannochloropsis salina* (*N. salina*) (Solix Biosystems, Inc), 6.75 g of α-D-glucose (Aldrich), and 70 mL of DI water were mixed together and stirred to obtain a uniform slurry. The mixture was then transferred into a ~100 mL Teflon lined stainless steel autoclave. After keeping the sealed autoclave at 473 K in an oven for 24 hour, a brownish HTC sample was separated by filtration, washed thoroughly with copious amounts of DI water several times, and dried at 353 K in a vacuum oven (denoted as HA, which stands for hydrothermally carbonized algae). Then the dry HA was chemically activated at 873 K for 1 h under a nitrogen atmosphere by physically mixing pulverized KOH (Fisher Chemical) with the weight ratio of KOH/HA = x (x = 0.5, 1, 2, or 4). The activated HA was thoroughly washed with copious amounts of DI water until neutral pH was reached and then dried at 373 K in a vacuum oven overnight (denoted as NAHA-x). The dry HA that was directly pyrolyzed at 873 K for 1 h under nitrogen protection (without chemical activation) was used here as a reference sample (denoted as PHA).[57]

2.2 Characterization of materials

The morphology of the as-made carbon samples was investigated using an S–3400N Type II scanning electron microscope (SEM). The elemental (C, H, and N) analyses were determined using a Perkin Elmer 2100 Series II combustion analyser. X-ray photoelectron spectroscopy (XPS) measurements were performed using a Kratos Amicus/ESCA 3400 instrument. The samples were irradiated with 240 W unmonochromated Mg Kα x-rays. All spectra were energy calibrated by setting C 1s to 284.6 eV. The textural properties of all the samples were assessed *via* the nitrogen adsorption/desorption isotherms at 77 K obtained on a Micromeritics ASAP 2020 volumetric sorptometer (the sample mass used was greater than 0.22 g). Prior to the adsorption measurements, the samples were degassed using a high vacuum pump (Pfeiffer Vacuum, model: MVP 015-2) at 473 K for over 12 h. The apparent Brunauer–Emmett–Teller (BET) specific surface area (S_{BET}) was calculated using the adsorption branch with the relative pressure P/P_0 in the range of 0.005 to 0.1. The total pore volume (V_{tot}) was measured based on the adsorbed amount of nitrogen at the P/P_0 of 0.99. The total micropore volume (pore width < 2 nm) V_{mic} and the narrow micropore volume (pore width < 0.7 nm) V_n were deduced from N_2 sorption isotherms at 77 K and CO_2 sorption isotherms at 273 K, respectively, by means of the Dubinin–Radushkevich (D–R) equation. The pore size distribution (PSD) was calculated using the non-local density functional theory (NL-DFT) methodology with nitrogen adsorption isotherm data and assuming a slit pore model.

2.3 Gas adsorption measurements

The adsorption/desorption equilibrium isotherms of CO_2, CH_4, C_2H_6, and H_2 at 273, 298, and 323 K were measured volumetrically by using a Micromeritics ASAP 2020 for pressures up to 100 kPa. The H_2 isotherms at 77 K (liquid nitrogen bath) and 87 K (liquid argon bath) were performed on a Micromeritics ASAP 2050. As aforementioned, samples were outgassed at 473 K under high vacuum for over 12 h prior to the adsorption measurements.

3 Results and discussion

3.1 Properties of the adsorbents

The morphologies of hydrothermally carbonized *N. salina* and its derivatives that were subjected to different treatments were investigated by scanning electron microscopy and the representative SEM images are displayed in Fig. 1. Sample HA is predominately composed of discrete spheres and irregular-shaped particles (such as broken, deflated, or deformed spheres) with rough surfaces and wide size distributions (Fig. 1a and b). It is worth noting that this morphology is, to some extent, different from the ones obtained from saccharides (*e.g.* glucose, cellulose, and starch) under similar hydrothermal conditions,[57–59] presumably because *N. salina* contains

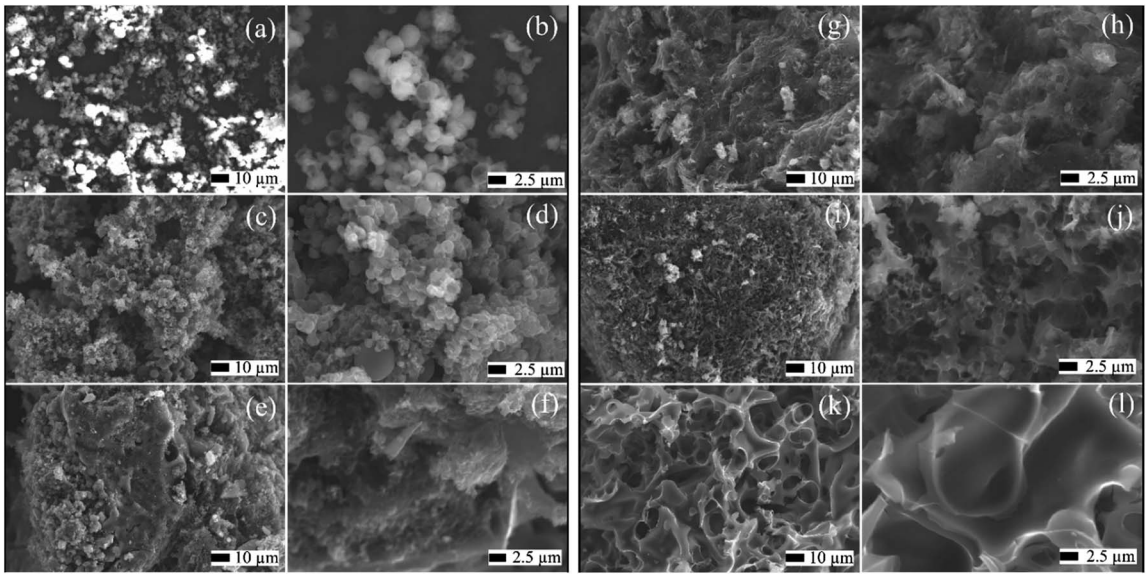

Fig. 1 SEM images of HA (a and b), PHA (c and d), NAHA-0.5 (e and f), NAHA-1 (g and h), NAHA-2 (i and j), and NAHA-4 (k and l).

a relatively low level of carbohydrates.[56,60] The pristine morphology of HA was preserved after pyrolysis (Fig. 1c and d), in accordance with previous results.[57] However, it was gradually destroyed by KOH activation as the weight ratio of KOH/HA increased from 0.5 to 4, as shown in Fig. 1e to g. Specifically, a morphologic evolution from discrete particles with rough surfaces (Fig. 1a and b) to granular monoliths (Fig. 1e–h), to monoliths with smooth surfaces and very sharp edges and corners (Fig. 1i–l) was observed, which is in good agreement with the reported result that KOH activation can lead to severe destruction of morphology.[51]

Nitrogen adsorption isotherms at 77 K were determined in order to probe the porosity of the carbons prepared under different conditions. As shown in Fig. 2, the hydrochar from *N. salina* is basically nonporous as sample HA has a negligible overall nitrogen adsorption uptake. Interestingly, hydrochar pyrolyzed at 873 K for 1 h (*i.e.* sample PHA) exhibits a sharp and major nitrogen adsorption at a low relative pressure range (P/P_0) (below 0.001), which is indicative of the development of microporosity owing to the release of volatiles caused by the thermal decomposition of hydrothermal carbon. Unsurprisingly, the profiles of the low temperature nitrogen sorption isotherms of all the KOH activated hydrothermal carbons are of typical type I (according to the IUPAC classification[61]) that reached a high adsorption plateau at a significantly low relative pressure, strongly suggesting a microporous feature of all the porous carbons prepared in this work. It is interesting to note that the knee of the nitrogen sorption isotherms gradually became wider as the KOH/HA ratio increased. This indicates a steady widening of the micropore size accompanied by a progressive broadening of the corresponding micropore size distribution of the porous carbons as confirmed by the PSD curves in Fig. 3. The nitrogen uptake at a high relative pressure ($P/P_0 > 0.9$) could be attributed to the interparticle space. A marginal extent of hysteresis was observed and could be explained by (i) slight unequilibrium of the obtained nitrogen sorption isotherms under the measurement conditions (*i.e.* equilibrium time),[57] and (ii) the presence of some mesopores (Table 1).

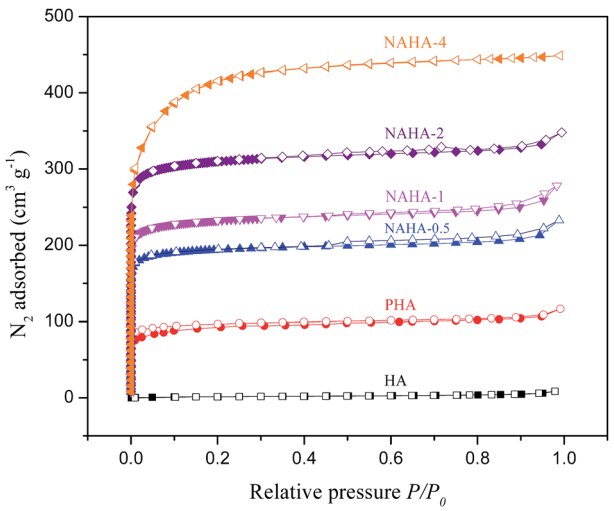

Fig. 2 N_2 sorption isotherms at 77 K of the as-made carbons.

The textural properties of the as-made carbons are summarized in Table 1. It can be seen from the sample PHA that modest specific surface area and pore volume were developed by mere pyrolysis. In contrast, KOH activation allowed a drastic increase in the values of the porosity parameters even with the weight ratio of KOH/HA = 0.5. Particularly, the KOH activated carbons show high apparent specific surface areas S_{BET} as well as pore volumes V_{tot} in the range of 747–1538 $m^2 g^{-1}$ and 0.36–0.69 $cm^3 g^{-1}$, respectively. As indicated in Table 1, S_{BET}, V_{tot}, and V_{mic} increased with the harshness of the activation condition (*i.e.* the KOH/HA ratio), approximately doubled when KOH/HA reached 4. However, a further increase of KOH dosage may lead

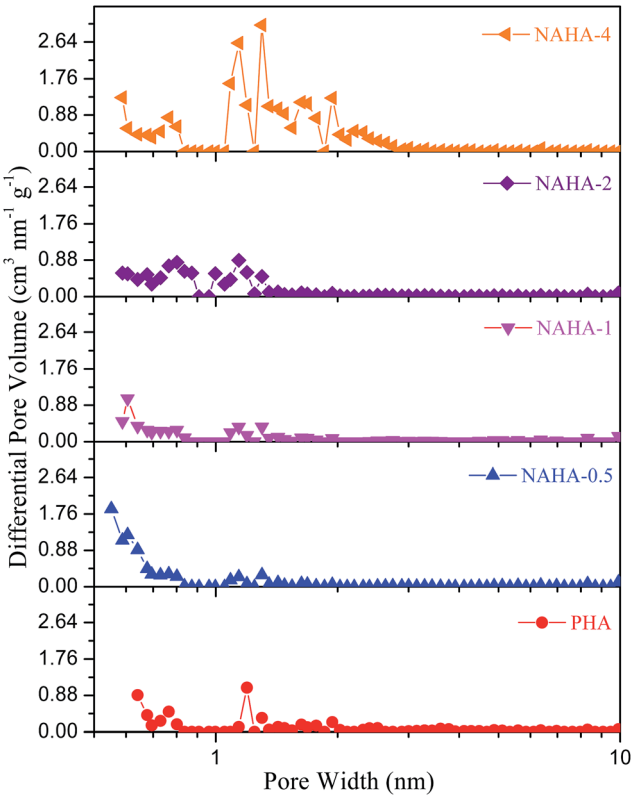

Fig. 3 NL-DFT pore size distributions for the as-prepared carbons derived from nitrogen adsorption at 77 K.

to a decrease in S_{BET} and V_{tot} as a result of destruction of existing pores.[62] Moreover, the porous carbons exhibit a very large proportion of V_{mic} (>81%), suggesting again their microporous nature. It is important to note that the existence of some mesopores (Table 1) can facilitate the diffusion of adsorbate molecules and consequently boost the rate of adsorption. Since the narrow micropore volume (pore width < 0.7 nm) has a significant effect on gas uptake (*e.g.* CO_2),[63] it was also calculated based on CO_2 adsorption isotherms at 273 K and is presented in Table 1. The variation of the narrow micropore volume V_n with KOH dosage was that: it first increased along with KOH dosage to a maximum and then started to decline with further increasing KOH dosage. In addition, the value of V_n minus V_{mic} changes from a negative number at low KOH dosage to a positive number when the weight ratio of KOH/HA $\geq$ 2, which evidently reveals the evolvement of the pore size of the porous carbon as the KOH dosage was increased: from primarily narrow micropores to micropores with supermicroporosity (pore width between 0.7 and 2 nm),[64] as evidenced by the PSD curves (Fig. 3) and the widening of the knee of the N_2 sorption isotherms (Fig. 2).

Table 1 Textual properties and the N content of pyrolyzed and activated carbons

Sample	S_{BET}[a] (m^2 g^{-1})	V_{tot}[b] (cm^3 g^{-1})	V_{mic}[c] (cm^3 g^{-1})	V_n[d] (cm^3 g^{-1})	N (wt%)
PHA	284	0.18	0.13 (72)	0.15 (83)	4.53
NAHA-0.5	747	0.36	0.29 (81)	0.30 (83)	3.25
NAHA-1	895	0.43	0.35 (81)	0.36 (84)	2.74
NAHA-2	1192	0.54	0.48 (89)	0.44 (81)	1.23
NAHA-4	1538	0.69	0.57 (83)	0.30 (43)	0.84

[a] Apparent specific BET surface area calculated in the P/P_0 range of 0.005 to 0.1. [b] Total pore volume at $P/P_0 \approx 0.99$. [c] Micropore volume determined from nitrogen adsorption isotherms at 77 K using the D–R equation; the values in the parentheses are the percentages of the micropore volume with respect to the total pore volume. [d] Narrow micropore volume obtained from CO_2 adsorption isotherms at 273 K using the D–R equation; the values in the parentheses are the percentages of the narrow micropore volume with respect to the total pore volume.

Besides tailoring the textural properties of the carbons by direct chemical activation with different extents of severity, general alternative approaches to enhance their adsorptive capability are to increase the adsorbate–adsorbent interaction, among which the incorporation of nitrogen into the carbonaceous framework has been demonstrated to be beneficial in this regard and received growing interest although the mechanism remains controversial.[65,66] In this work, N-containing carbons were prepared directly by using the nitrogen-rich precursor (*N. salina*) instead of by post-synthetic treatment with N-containing chemicals (*e.g.* ammonia and amines),[67] as the carbons prepared by the latter method have been reported to have a few serious disadvantages, such as lacking stability and having compromised porosity and gas uptake capacity.[42,68–70] The nitrogen content of the carbon adsorbents is listed in Table 1. PHA, as expected, has the highest nitrogen content of 4.53 wt%. As also can be seen, the nitrogen content in the activated carbon matrix decreases evidently with the increase in KOH dosage, ranging from 3.25 wt% for sample NAHA-0.5 to 0.84 wt% for sample NAHA-4. This result shows that there is a trade-off between the two critical adsorptive parameters of the activated carbons, *i.e.* the nitrogen content and the surface area (or pore volume) whose effect on gas adsorption and separation will be discussed in detail later.

The adsorption and separation performance of an adsorbent is closely related to its surface chemical properties. It is well known that N-functional groups can enhance the CO_2 adsorption capacity and selectivity *via* different mechanisms (*e.g.* acid–base interaction and hydrogen-bonding).[66] Very recently, the correlation between CO_2/N_2 selectivity and one type of nitrogen species (pyrrolic-N) has been reported.[71] Herein, in order to explore the relationship between gas adsorption capacity/selectivity and nitrogen types, in addition to the determination of the total nitrogen amount by CHN elemental analysis, the nature of the nitrogen functionalities in all the as-synthesized porous carbons was studied by XPS. As presented in Fig. 4, the nitrogen species and their proportions on the surface of different carbons are significantly different. The N 1s XPS spectrum of PHA can be deconvoluted into three peaks at 400.5, 398.4, and 402 eV which are generally attributed to pyridonic/pyrrolic-N, pyridinic-N, and oxidized-N, respectively.[72] This is in agreement with previous results for carbons obtained under similar pyrolysis conditions.[73] For NAHA-0.5, three intense peaks at 400.0, 398.2, and 401.4 eV could be distinguished and

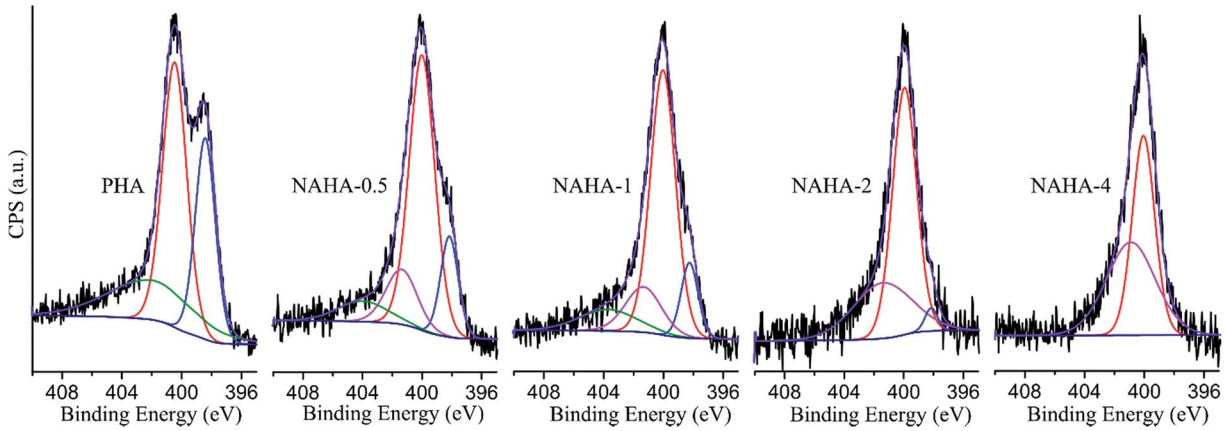

Fig. 4 N 1s XPS spectra of the as-prepared carbons.

assigned to pyridonic/pyrrolic-N, pyridinic-N, and quaternary-N, respectively, similar to that previously reported for activated carbon.[52,74] Besides, a weak broad peak (centered at ~404 eV) corresponding to the oxidized-N was also revealed by XPS in NAHA-0.5 and NAHA-1. As shown in Fig. 4, the proportion of pyridinic-N decreases from 15% to 0 and the proportion of quaternary-N increases from 15% to 50% as the severity of the activation condition, *i.e.* the KOH/HA ratio, increases from 0.5 to 4. A similar trend has also been reported in the literature with increasing the severity of activation condition.[71,75,76] It should be noted that the pyridonic/pyrrolic-N is the main type of nitrogen species in all the samples. Because pyridonic-N and pyrrolic-N cannot be distinguished by XPS and both of them are much more effective for CO_2 adsorption than other forms of nitrogen (*e.g.* pyridinic and quaternary),[77–79] no differentiation between them will be made here, although it is more likely that pyridonic-N was formed in our samples under the activation conditions.[52,80] The percentage of nitrogen atoms in the form of pyrrolic/pyridonic-N with respect to all the atoms (C, O, and N) in the sample determined by XPS is shown in Fig. S1.† This percentage is denoted as Np% here. It can be seen in Fig. S1† that the Np% in PHA is almost identical to the one in NAHA-0.5. More importantly, the Np% decreases monotonically from 1.83% to 0.92% with the increase of KOH/HA ratio from 0.5 to 4. This trend is analogous to the trend that the N content determined by elemental analysis is inversely correlated with the KOH/HA ratio (Table 1). Therefore, for the as-made activated carbons, the correlation between the Np% and the gas adsorption capacity/selectivity, if any, should be consistent with the correlation between the total N content and the gas adsorption capacity/selectivity. The presence/absence of the correlation will be discussed later. It should be pointed out that the influence of other types of nitrogen species (pyridinic and quaternary) is ignored here.[81]

3.2 Gas adsorption analysis

Fig. 5 shows the volumetric pure component (CO_2, C_2H_6, CH_4, and H_2) adsorption isotherms of the carbonaceous materials studied at 273 K and pressure up to 100 kPa. All the isotherms are reversible with no hysteresis as revealed by the representative adsorption and desorption isotherms of CO_2, C_2H_6, CH_4, and H_2 on the pyrolyzed carbon (PHA) and the activated porous carbon (NAHA-0.5) (Fig. S2a and b in the ESI†), indicating that (i) the sorption of the gases is a physical or weak chemical adsorption process despite the presence of nitrogen content in the carbon framework and (ii) the adsorbents can be easily regenerated. The initial slopes of the isotherm profiles follow the order $C_2H_6 > CO_2 > CH_4 > H_2$ due to the fact that the strength of the interaction between the gas molecule and adsorbent follows the same order, as indicated by the isosteric heat of adsorption that will be discussed later.

As the focus of this study is the separation of CO_2 from CH_4, CO_2 from H_2, and C_2H_6 from CH_4, the uptake capacity of CO_2 and C_2H_6 on the carbons is one of the key parameters that must be considered for the evaluation of the separation performance.

In the case of C_2H_6 adsorption, the pyrolyzed hydrothermal carbon (PHA) shows the smallest C_2H_6 uptake at 273 K and 100 kPa (1.7 mmol g^{-1}) owing to its poorest porosity development. Clearly, all the activated hydrothermal carbons present substantially higher C_2H_6 uptake capacity in the range of 3.6–5.8 mmol g^{-1}. Similarly, in the case of CO_2 adsorption, the amount of adsorbed CO_2 at 273 K and 100 kPa on PHA is the lowest (2.1 mmol g^{-1}). KOH activation led to evidently a higher CO_2 uptake that is in the range of 4.6–6.0 mmol g^{-1}.

A comparative analysis shows that the sequence of CO_2 uptake capacity at 273 K and 100 kPa (NAHA-2 > NAHA-4 > NAHA-1 > NAHA-0.5) is inconsistent with the order of the total surface area (or total pore volume, or micropore volume) of the activated porous carbons. Specifically, while NAHA-4 has the highest total surface area among all the activated carbons, its CO_2 adsorption capacity is lower than that of NAHA-2 and comparable to that of NAHA-1. Moreover, it can be seen from Fig. 5 that although the C_2H_6 uptake of the activated carbons at 100 kPa increases with the total surface area, it is not always the case in the whole pressure range measured. These observations suggest that other factors (*e.g.* narrow micropore volume, total N content, and Np%) rather than the total surface area may be the overriding factors for the gas adsorption behaviour under certain circumstances.

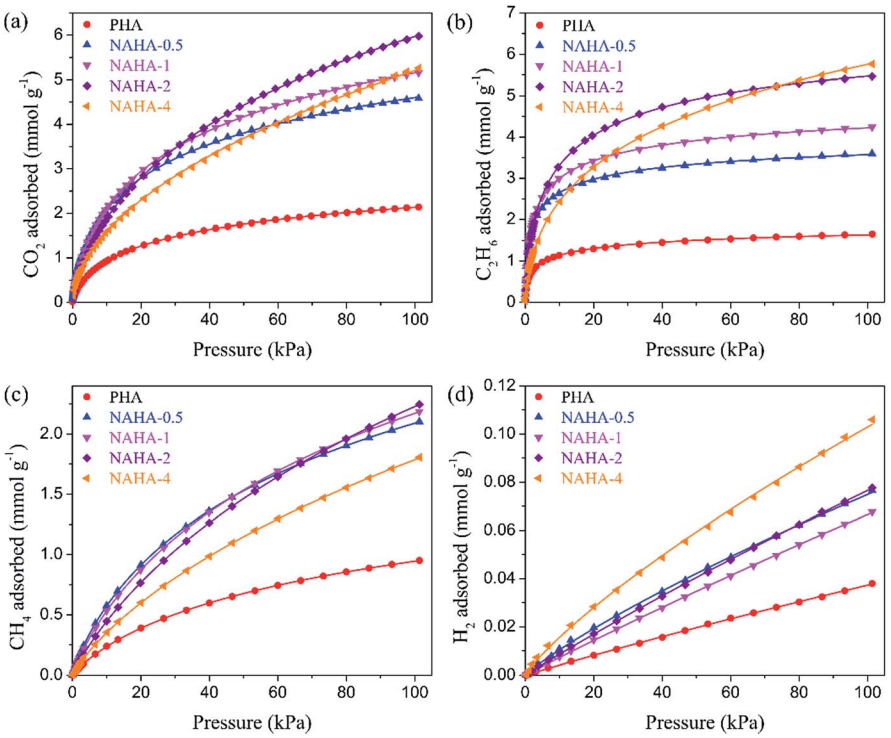

Fig. 5 CO_2 (a), C_2H_6 (b), CH_4 (c), and H_2 (d) adsorption isotherms of the various carbons at 273 K. The lines represent Toth isotherm fitting.

A further careful study of the isotherms indicates that the CO_2 adsorption isotherms of the activated porous carbons can be divided into four regions (Fig. 6) on the basis of the following criteria. Region 1 is the maximum region within which the CO_2 uptake has the order of NAHA-0.5 > NAHA-1 > NAHA-2 > NAHA-4; the separation of regions 2 and 3 is the point where NAHA-0.5 and NAHA-4 have identical CO_2 uptake. This point was selected based on the fact that NAHA-0.5 and NAHA-4 have the same narrow micropore volume V_n. The separation point for regions 3 and 4 is the one at which NAHA-3 and NAHA-4 exhibit the same CO_2 uptake. These four regions allow better understanding of the respective effect of textural properties (S_{BET}, T_{tot}, V_{mic}, and V_n) and the nitrogen content (or Np%) on the gas adsorption uptake.

At the initial stage of the adsorption (region I), the CO_2 adsorption could be partially attributed to the N content and/or Np% as: (i) it has been well documented that the adsorption of CO_2 at low pressures heavily relies on the surface chemistry of the adsorbents (*i.e.* doped N here);[82,83] (ii) the order of CO_2 uptake is consistent with the order of N content and Np%. The influence of N content and Np% on CO_2 adsorption is further confirmed by the behaviour that higher N content and Np% resulted in a higher isosteric heat of adsorption of CO_2 which will be discussed in detail later. It should be pointed out that the low pressure gas uptake may also be partially attributed to the volume of very small micropores.[74,84,85] In region II, CO_2 uptake on the sample NAHA-2 that has a low N content and

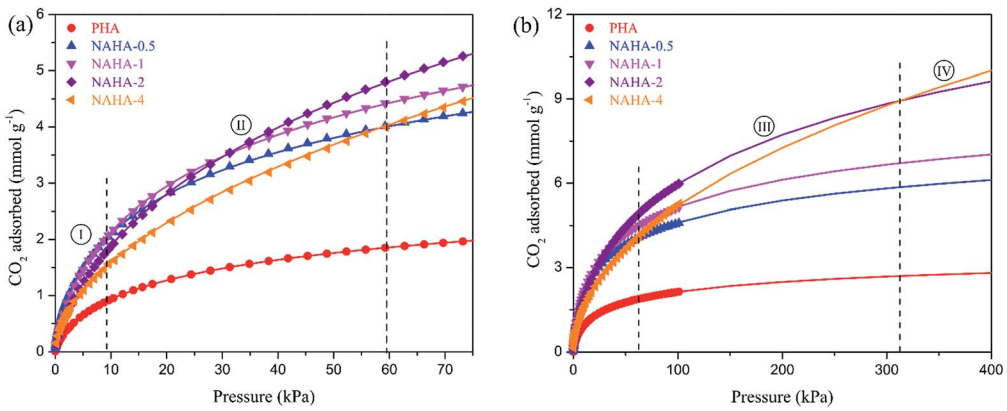

Fig. 6 CO_2 adsorption isotherms of the investigated carbons at 273 K. The lines represent Toth isotherm fitting. Data above 100 kPa were obtained by extrapolating the fitted Toth isotherm curves.

Np% but the highest narrow micropore volume starts to catch up and exceed the CO_2 uptakes on all the other samples. Besides, the CO_2 isotherm profile of sample NAHA-4 that has a narrow micropore volume equal to that of NAHA-1 but the least N content (and least Np%) converges with the profile of sample NAHA-1. A conclusion can be drawn from the observed behaviour that in region II the narrow micropore volume plays a significant role in CO_2 adsorption due to the fact that narrow micropores have a great adsorption potential. In region III, the bottom isotherm curve from sample NAHA-4 that has the least N content (and least Np%) and narrow micropore volume rises up, crosses other isotherms and becomes the top isotherm in region IV. The resulting order of CO_2 uptake in region IV follows the order of surface area and pore volume. This result reveals that the surface area and pore volume have a greater effect on CO_2 uptake than others at high pressure (in regions III and IV).

Interestingly, the isotherm configuration of C_2H_6 at 273 K is analogous to the above-mentioned configuration of CO_2 and can also be split into similar four parts (Fig. S3 in the ESI†). Consequently, it can be deduced that both N incorporation and the narrow micropore volume play a vital role in the enhancement of C_2H_6 adsorption. The former is explainable considering that N doping can increase the surface polarity of adsorbents,[67] and then increase both the probability and strength of interaction between the adsorbents and C_2H_6 that has high polarizability (4.5×10^{-24} cm^3) and moderate quadruple moment (2×10^{-40} C m^2).[86] The latter is reasonable in light of the fact that narrow micropores have a high adsorption potential due to the overlapping of the dispersion forces from the neighboring walls of the narrow micropores. To the best of our knowledge, this is the first example indicating the positive effect of N doping and narrow micropore volume on the adsorption of C_2H_6. This finding could be of great importance for the design of suitable adsorbents for C_2H_6 adsorption.

We also explored the influence of the same parameters (N content and Np%, V_n, and S_{BET}) on the adsorption of H_2 and CH_4. As the H_2 isotherm at 273 K is linear, the influence of the parameters is too weak to be noticed. Therefore, we measured the H_2 adsorption isotherms at 87 K (Fig. S4 in the ESI†). Although the H_2 and CH_4 isotherm configurations show similar four regions (Fig. S4 and S5†), there is a significant difference regarding the influence of parameters on the gas uptake: the impact of N doping on the H_2 and CH_4 adsorption is negligible as the isosteric heats of adsorption on NAHA-1 (total N doping = 2.74 wt% and Np% = 1.68%) and NAHA-2 (total N doping = 1.23 wt% and Np% = 1.04%) are almost the same for H_2 and CH_4, whereas they are significantly lower on NAHA-2 than the ones on NAHA-1 for CO_2 and C_2H_6 (discussed later). This significant difference is expected to produce a remarkable CO_2/CH_4, CO_2/H_2, and C_2H_6/CH_4 selectivity.

Samples NAHA-1 and NAHA-2 were chosen as typical examples to further investigate the dependency of adsorption performance on temperature since they have a good combination of N doping level, narrow micropore volume, and total surface area. The CO_2, C_2H_6, and CH_4 isotherms on the two selected carbons and the reference material (PHA) at 273, 298, and 323 K are illustrated in Fig. 7, S6, and S7† (these isotherms will also be used to calculate heat of adsorption and temperature-dependent selectivity later on). As the H_2 uptake is already very low (<0.1 mmol g^{-1}) at 273 K and 100 kPa, its isotherms at cryogenic temperatures (77 and 87 K) on NAHA-1 and NAHA-2 were measured instead and presented in Fig. S6 and 7,† respectively. It can be observed that the gas uptake diminishes with the increase of temperature due to the exothermic feature of the sorption process. Importantly, as shown in Table S1,† the CO_2 uptakes on NAHA-2 at 273 K (6.0 mmol g^{-1}) and 298 K (4.0 mmol g^{-1}) are among the highest ever reported for carbon-based adsorbents. For example, they are superior to the ones achieved on commercial activated carbons,[87] comparable to those obtained on N containing polypyrrole-based carbon,[76] and close to the values reported on activated hydrothermal carbon from sawdust.[51] They are also higher than the reported values for amine-grafted SBA-15,[88] zeolite 13X,[89] and NU-100 that exhibited huge surface area.[36] In addition, the C_2H_6 uptake capacity of NAHA-2 at 273 K (5.5 mmol g^{-1}) and 298 K (4.6 mmol g^{-1}) outperforms all the reported values for various carbons except for the recently reported zeolite-template carbon and Maxsorb MSC-30,[90] to the best of our knowledge (Table S2†). Besides the gravimetric adsorption capacity, the volumetric adsorption capacity is also critically important from a practical point of view as it can influence the volume of the adsorbent bed.[35,91] By assuming a packing density of 0.5 g cm^{-3}, the volumetric adsorption capacities were determined. At 100 kPa and 298 K, the volumetric capacity of CO_2 and C_2H_6 is 1.89 mmol cm^{-3} (42.3 cm^3 cm^{-3}) and 1.83 mmol cm^{-3} (40.9 cm^3 cm^{-3}), respectively, on NAHA-1, and 2.01 mmol cm^{-3} (44.9 cm^3 cm^{-3}) and 2.31 mmol cm^{-3} (51.7 cm^3 cm^{-3}), respectively, on NAHA-2. The estimated CO_2 volumetric adsorption capacities are superior to the ones reported on some activated carbons and MOFs: AC-1 and Max3 (~1.2 mmol cm^{-3}),[92] MOF-205-OBn (~0.4 mmol cm^{-3}),[93] Zn(bdc)(dabco) (~1.7 mmol cm^{-3}),[35] MIL-101 (~1 mmol cm^{-3}),[35] and MOF-177 (~0.5 mmol cm^{-3}).[35] The assumed packing density (0.5 g cm^{-3}) could be practically achievable without significantly changing the porosity of the as-prepared carbons as (i) the general packing density reported in the literature for activated carbon is in the range of 0.4–0.9 g cm^{-3} and (ii) a higher packing density of 0.6 g cm^{-3} can be achieved without significantly compromising the porosity.[5,94–96]

3.3 Isosteric heats of adsorption

Isosteric heat of adsorption (Q_{st}) is widely used to determine the interaction strength between the adsorbate molecules and adsorbent surface, and to probe the surface heterogeneity of the adsorbents. It is also very important for practical application as temperature variation can drastically affect the adsorption and separation performance. Besides, it reflects the preferential adsorption of C_2H_6 and CO_2 over CH_4 and H_2 and demonstrates the effect of N-doping on gas adsorption here. All the adsorption isotherms were fitted by the Toth equation (see the ESI†) for the calculation of Q_{st} and selectivity (discussed in the next section). The best fitting parameters are compiled in Table S3 in the ESI.† The Toth model fits the isotherms very well in the entire studied pressure range as shown in Fig. 5 and 7, S6, and S7,† and it is

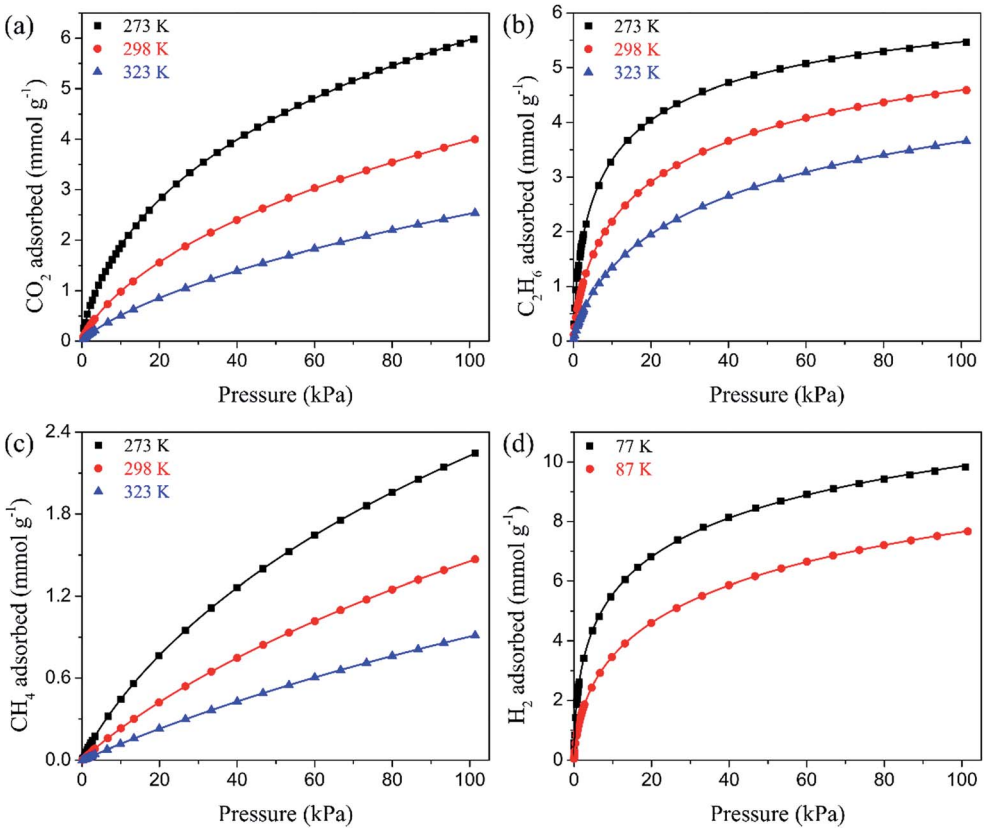

Fig. 7 CO_2 (a), C_2H_6 (b), and CH_4 (c) isotherms of NAHA-2 at 273, 298, and 323 K. H_2 (d) isotherms of NAHA-2 at 77 and 87 K. The lines represent Toth isotherm fitting.

better than Langmuir and virial equations. The Q_{st} for the pure-component adsorption was determined by applying the Clausius–Clapeyron equation to the adsorption isotherms collected at different temperatures (Q_{st} of C_2H_6, CO_2, and CH_4 was calculated using isotherms at 273, 298, and 323 K and Q_{st} of H_2 was evaluated using isotherms at 77 and 87 K).

The dependence of Q_{st} on surface coverage for NAHA-2, NAHA-1, and PAH is presented in Fig. 8 and S8.† There is a general descending trend for Q_{st} with the increase of surface loading, indicating that the carbons have energetically heterogeneous surfaces. Generally, surface chemistry and textural properties (*e.g.* pore size and surface area) are two of the most important factors that substantially affect the heat of adsorption. The result that NAHA-1 showed significantly higher Q_{st} for C_2H_6 and CO_2 in relation to NAHA-2 (Fig. 8) may be primarily attributed to the higher level of total nitrogen and/or Np% in NAHA-1 rather than the smaller pore size of NAHA-1. This is supported by the fact that sample PHA that had the highest N content and Np% among the three samples but a slightly wider pore size than that of NAHA-1 (Fig. 3) showed the highest Q_{st} for C_2H_6 and CO_2 (Fig. S8†). In contrast, the N content and Np% have an insignificant effect on the Q_{st} of CH_4 and H_2 as the Q_{st} of CH_4 and H_2 on NAHA-1 and NAHA-2 are approximately the same. The slight difference can be presumably attributed to the difference in their textural properties. It was previously reported that N-doping can have some effects on the Q_{st} of H_2.[5,67] Here the insignificant effect of N-doping on the Q_{st} of H_2 and CH_4 could be due to the relatively low levels of N-doping. The selective enhancement of the heat of adsorption of C_2H_6 and CO_2 by N-doping again predicts the high selectivity for separation of C_2H_6/CH_4, CO_2/CH_4, and CO_2/H_2 mixture pairs.

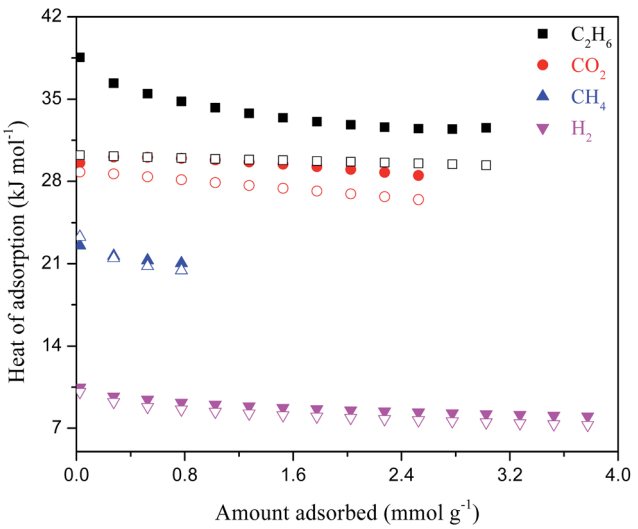

Fig. 8 Isosteric heat of adsorption for NAHA-1 (filled symbols) and NAHA-2 (open symbols) at different gas loadings.

The Q_{st} values of C_2H_6 on NAHA-1 and NAHA-2 lie in the range of 29.4–38.5 kJ mol^{-1} (surface loading between 0.025 and 3 mmol g^{-1}), which are comparable to or higher than those typically reported for activated carbons[97–99] and some well-known MOFs.[21,100,101] NAHA-1 and NAHA-2 exhibit high Q_{st} values for CO_2 varying from 26.4 to 30.1 kJ mol^{-1} (surface loading between 0.025 and 3 mmol g^{-1}). These values exceed the ones found on pure carbon materials[102] and are in line with the values reported for N-doped carbons.[73,76]

3.4 Selectivity for separation of C_2H_6/CH_4, CO_2/CH_4, and CO_2/H_2 binary mixtures

As mentioned earlier, selectivity is one of the two most important criteria to assess the separation performance of an adsorbent. Here, in order to assess the performance of the activated hydrothermal carbons with regard to the greenhouse gas capture and clean energy purification, we proceeded to investigate the selectivities for the binary mixtures of C_2H_6/CH_4, CO_2/CH_4, and CO_2/H_2. The selectivities were determined using the ideal adsorbed solution theory (IAST)[103] which has been extensively and successfully applied to carbons and other adsorbents (*e.g.* MOFs and zeolites). The parameters (Table S3†) obtained by fitting the pure-component adsorption isotherms with the Toth model were used to perform the IAST calculation (see the ESI†).

Fig. 9 shows the IAST predicted selectivities for the three binary mixtures at 273 K as a function of bulk pressure and mixture composition. (i) In the case of C_2H_6/CH_4 selectivity: the selectivity of the equimolar binary mixture decreases as the pressure increases and gradually levels off as the pressure approaches the atmospheric pressure for all the carbons (Fig. 9a). NAHA-1 shows the highest C_2H_6/CH_4 selectivity over the entire pressure range ranging from 32.6 to 72.0. The selectivity of NAHA-0.5 is very close to that of NAHA-1. NAHA-2 and NAHA-4 exhibit lower C_2H_6/CH_4 selectivity varying over the ranges of 23.9–42.6 and 18.4–36.7, respectively. In contrast, C_2H_6/CH_4 selectivity increases with the gas phase mole fraction of CH_4 (Fig. 9d). (ii) In the case of CO_2/CH_4 selectivity: the selectivity of the equimolar binary mixture initially decreases then does not vary much with the increase of pressure (Fig. 9b). At 100 kPa, the selectivities for the equimolar binary CO_2/CH_4 mixture on NAHA-0.5 to NAHA-4 are 11.2, 10.4, 8.0, and 9.0, respectively. Moreover, the CO_2/CH_4 selectivity shows a weak dependence on the gas phase mole fraction of CH_4 in every investigated carbon (Fig. 9e). It should be pointed out here that a sorbent with a high selectivity that is almost independent on bulk pressure and mixture composition is highly demanded for industrial applications because it can separate a gas mixture at any desired bulk pressure and mixture composition. (iii) In the case of CO_2/H_2 selectivity: the selectivities for the equimolar CO_2/H_2 binary mixture in NAHA-0.5 and NAHA-4 diminish with increasing pressure, whereas they keep increasing with pressure in all other as-prepared carbons (Fig. 9c). The increase in CO_2/H_2 selectivity with pressure is an excellent property for an adsorbent as pre-combustion CO_2 capture is normally carried out under a high pressure (*e.g.* 3000 kPa). Although the CO_2/H_2 selectivities of PHA, NAHA-1, and NAHA-2 monotonically decrease with the gas phase mole fraction of H_2, they are still extraordinarily high (>840) even at a 5/95 CO_2/H_2 ratio (Fig. 9f). For a typical CO_2/H_2 ratio of syngas after the water–gas shift reaction, *i.e.* $CO_2/H_2 = 40/60$, NAHA-1 has a CO_2/H_2 selectivity over 10^4 at 273 K, 100 kPa.

Based on the isotherms collected for the two representative samples and the reference sample at different temperatures as shown in Fig. 7, S6, and S7,† we further explored the temperature dependence of C_2H_6/CH_4 and CO_2/CH_4 selectivity for the corresponding equimolar binary mixtures (Fig. S9†). As shown in Fig. S9c and d,† the C_2H_6/CH_4 and CO_2/CH_4 selectivities of NAHA-1 at 298 K are in the range of 23.7–44.9 and 7.0–9.0, respectively.

To highlight the outstanding C_2H_6/CH_4, CO_2/CH_4, and CO_2/H_2 separation performance (uptake capacity and selectivity) of the activated hydrothermal carbons prepared in this study, we compare them with the ones obtained on other carbons (Table S4†) and the ones reported on other kinds of sorbents (*e.g.* MOFs, zeolites, clays, and ordered mesoporous silica) (Table S5†). (i) Compared with other carbons, NAHA-1 has the best C_2H_6/CH_4 and CO_2/H_2 equilibrium separation performance among carbons under similar conditions because it exhibits both the highest C_2H_6/CH_4 and CO_2/H_2 selectivities and exceptional C_2H_6, CO_2 uptake capacities, to the best of our knowledge. For example, its C_2H_6 uptake capacity (3.7 mmol g^{-1} at 298 K and 100 kPa) and C_2H_6/CH_4 selectivity (24–45 for the equimolar C_2H_6/CH_4 binary mixture at 298 K) are much higher than those of BPL carbon (uptake: 2.8 mmol g^{-1}, selectivity: ~17 under similar conditions).[97] Its CO_2 uptake capacity (5.2 mmol g^{-1} at 273 K and 100 kPa) and CO_2/H_2 selectivity (over 2×10^4 for the equimolar CO_2/H_2 binary mixture at 273 K) are also much higher than the ones reported on carbonized porous aromatic framework (uptake: 4.5 mmol g^{-1}, selectivity: <400 under same conditions).[104] For the CO_2/CH_4 separation, although NAHA-1 exhibits lower CO_2/CH_4 selectivity (9.7–10.7 at 273 K, 6.9–9.0 at 298 K) than the MOF derived carbon (8–13 at 273 K)[105] and the carbon prepared with the assistance of deep eutectic solvents (14.8 at 298 K),[106] it has much higher CO_2 uptake capacity. The CO_2/CH_4 separation performance of NAHA-1 is comparable to the one reported on the carbon prepared using ZIF-8 as a template and precursor[107] and much better than many other carbons, such as ordered mesoporous carbon,[108] and functionalized hierarchical porous carbon.[109] Taken together, NAHA-1 also has one of the best CO_2/CH_4 separation performances among carbons. It should be mentioned here that Henry's law selectivities reported in the literature (listed in Table S4 and S5†) are not considered here as they are generally larger than the IAST predicted values,[106] although the two selectivities should be identical in theory at pressures close to zero. (ii) Compared with other kinds of sorbents, C_2H_6/CH_4, CO_2/CH_4, and CO_2/H_2 separation performance of NAHA-1 is superior or comparable to those of many MOFs,[35,110,111] zeolites,[112,113] clays,[114,115] ordered mesoporous silica,[116,117] and others[118,119] under similar conditions. Detailed comparisons are presented in Table S5.† Furthermore, it is important to note that adsorbents that have such high

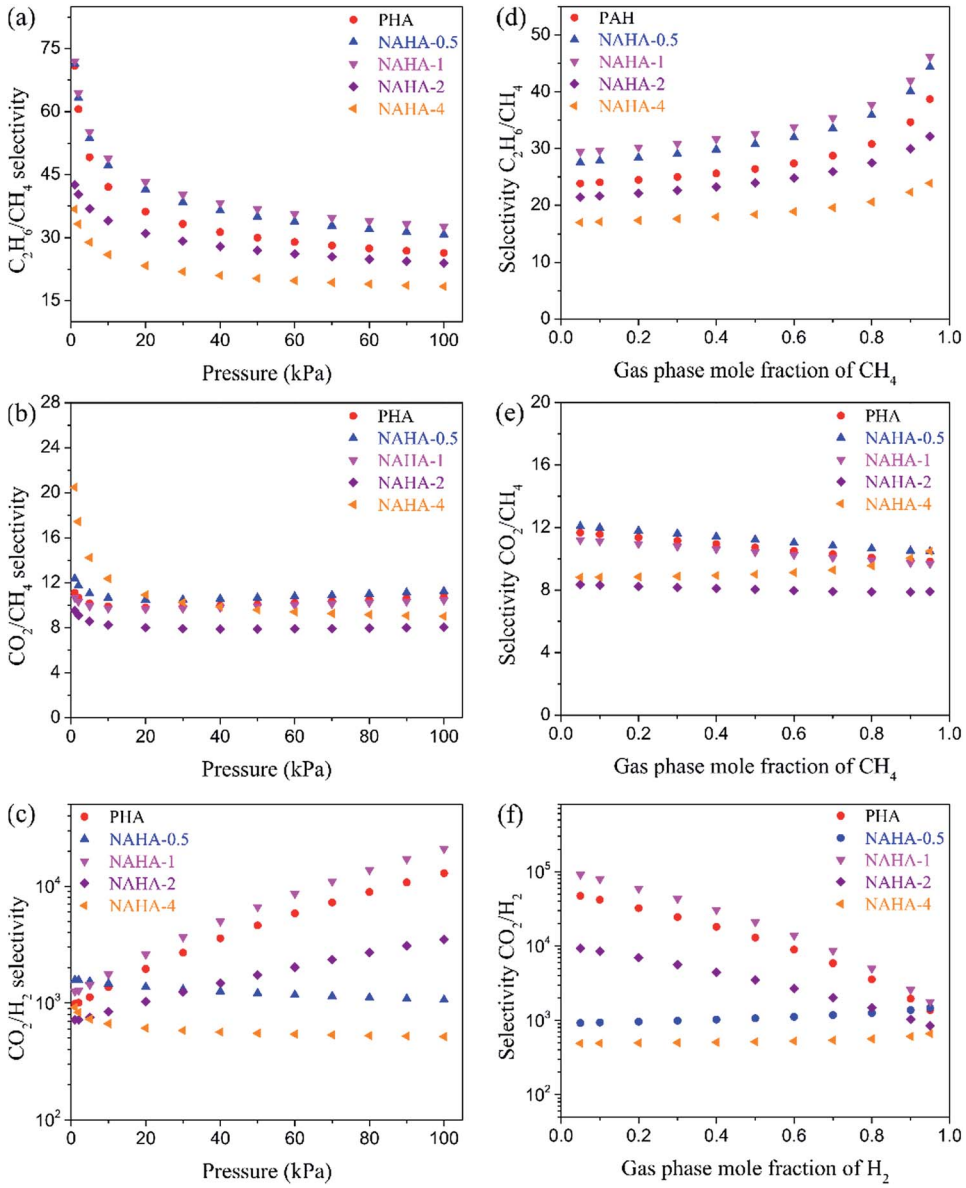

Fig. 9 IAST predicted selectivities for C_2H_6 over CH_4 (a and d), CO_2 over CH_4 (b and e), and CO_2 over H_2 (c and f) for the corresponding equimolar binary mixtures at 273 K as a function of bulk pressure (a, b and c), and for the corresponding binary mixtures at 273 K and 100 kPa as a function of mixture composition (d, e and f).

performance in the three aspects of separation (*i.e.* C_2H_6/CH_4, CO_2/CH_4, and CO_2/H_2) simultaneously are scarcely reported in the literature. The remarkable separation performance of NAHA-1 (and NAHA-2) could be attributed to the integrated effect of all the parameters (*i.e.* N content, narrow micropore volume, and total surface area). It is worth mentioning that, although N-doping can selectively increase the heats of adsorption of C_2H_6 and CO_2, there is no clear correlation between the N level (total N content and Np%) and selectivity. This is at least partially because selectivity is closely related to gas uptake capacity and gas uptake capacity does not only depend on heat of adsorption. As mentioned above, the gas uptake capacity under different pressures may be governed by different parameters. The influence of N doping (total N content and Np%) on the gas selectivity could be more clear if other parameters are kept the same for all the samples used for study which is very hard to achieve experimentally, if possible.

4 Conclusions

The foregoing results demonstrate that NAHA-1 and NAHA-2 have not only exceptional C_2H_6 and CO_2 adsorption uptake capacities but also remarkable selectivities for separating C_2H_6/CH_4, CO_2/CH_4, and CO_2/H_2 binary mixtures. Specifically, the equilibrium separation performance of NAHA-1 for the three binary mixtures is the best among various carbons reported in the literature and is superior or comparative to those reported on many MOFs and other adsorbents. These findings are of

great significance because the generally accepted opinion that carbons show inferior separation performance than other adsorbents (*e.g.* MOFs and zeolites) cannot stand here. Additionally, taking into account the fact that carbons can satisfactorily meet the aforementioned "inherent criteria", the N-doped activated hydrothermal carbons in this work were demonstrated to have a great potential in greenhouse-gas capture and clean energy applications. As a result, this study can potentially broaden the potential application of hydrothermal carbons.

Acknowledgements

This project was partially supported by US NSF through grants EEC 1028968 and #IIA-1301346, and the US DOE REAP project (DE-EE0006316).

Notes and references

1 N. von der Assen, P. Voll, M. Peters and A. Bardow, *Chem. Soc. Rev.*, 2014, **43**, 7982–7994.
2 M. E. Boot-Handford, J. C. Abanades, E. J. Anthony, M. J. Blunt, S. Brandani, N. Mac Dowell, J. R. Fernández, M.-C. Ferrari, R. Gross and J. P. Hallett, *Energy Environ. Sci.*, 2014, **7**, 130–189.
3 N. von der Assen, J. Jung and A. Bardow, *Energy Environ. Sci.*, 2013, **6**, 2721–2734.
4 J. M. Huck, L.-C. Lin, A. H. Berger, M. N. Shahrak, R. L. Martin, A. S. Bhown, M. Haranczyk, K. Reuter and B. Smit, *Energy Environ. Sci.*, 2014, **7**, 4132–4146.
5 M. Sevilla and R. Mokaya, *Energy Environ. Sci.*, 2014, **7**, 1250–1280.
6 M. Zhao, J. Shi, X. Zhong, S. Tian, J. Blamey, J. Jiang and P. S. Fennell, *Energy Environ. Sci.*, 2014, **7**, 3291–3295.
7 J. Yang, A. Sudik, C. Wolverton and D. J. Siegel, *Chem. Soc. Rev.*, 2010, **39**, 656–675.
8 J. Pang, F. Jiang, M. Wu, D. Yuan, K. Zhou, J. Qian, K. Su and M. Hong, *Chem. Commun.*, 2014, **50**, 2834–2836.
9 T. Remy, E. Gobechiya, D. Danaci, S. Peter, P. Xiao, L. van Tendeloo, S. Couck, J. Shang, C. Kirschhock and R. Singh, *RSC Adv.*, 2014, **4**, 62511–62524.
10 D. Ko, H. A. Patel and C. T. Yavuz, *Chem. Commun.*, 2015, 2915–2917.
11 M. Zhao, A. I. Minett and A. T. Harris, *Energy Environ. Sci.*, 2013, **6**, 25–40.
12 D. M. D'Alessandro, B. Smit and J. R. Long, *Angew. Chem., Int. Ed.*, 2010, **49**, 6058–6082.
13 K. Sumida, D. L. Rogow, J. A. Mason, T. M. McDonald, E. D. Bloch, Z. R. Herm, T.-H. Bae and J. R. Long, *Chem. Rev.*, 2011, **112**, 724–781.
14 A. S. Mestre, C. Freire, J. Pires, A. P. Carvalho and M. L. Pinto, *J. Mater. Chem. A*, 2014, **2**, 15337–15344.
15 E. Privalova, S. Rasi, P. Mäki-Arvela, K. Eränen, J. Rintala, D. Y. Murzin and J.-P. Mikkola, *RSC Adv.*, 2013, **3**, 2979–2994.
16 M. E. Casco, M. Martínez-Escandell, E. Gadea-Ramos, K. Kaneko, J. Silvestre-Albero and F. Rodriguez-Reinoso, *Chem. Mater.*, 2015, **27**, 959–964.
17 Y. He, W. Zhou, G. Qian and B. Chen, *Chem. Soc. Rev.*, 2014, **43**, 5657–5678.
18 L. Firlej, P. Pfeifer and B. Kuchta, *Adv. Mater.*, 2013, **25**, 5971–5974.
19 D. Wang, T. Zhao, Y. Cao, S. Yao, G. Li, Q. Huo and Y. Liu, *Chem. Commun.*, 2014, **50**, 8648–8650.
20 X. Su, P. Tian, D. Fan, Q. Xia, Y. Yang, S. Xu, L. Zhang, Y. Zhang, D. Wang and Z. Liu, *ChemSusChem*, 2013, **6**, 911–918.
21 E. D. Bloch, W. L. Queen, R. Krishna, J. M. Zadrozny, C. M. Brown and J. R. Long, *Science*, 2012, **335**, 1606–1610.
22 X. Duan, Y. He, Y. Cui, Y. Yang, R. Krishna, B. Chen and G. Qian, *RSC Adv.*, 2014, **4**, 23058–23063.
23 Y. He, W. Zhou, R. Krishna and B. Chen, *Chem. Commun.*, 2012, **48**, 11813–11831.
24 D. Li, M. Koike, L. Wang, Y. Nakagawa, Y. Xu and K. Tomishige, *ChemSusChem*, 2014, **7**, 510–522.
25 G. Li, H. Kobayashi, J. M. Taylor, R. Ikeda, Y. Kubota, K. Kato, M. Takata, T. Yamamoto, S. Toh and S. Matsumura, *Nat. Mater.*, 2014, **13**, 802–806.
26 S. Luo, L. Zeng, D. Xu, M. Kathe, E. Chung, N. Deshpande, L. Qin, A. Majumder, T.-L. Hsieh and A. Tong, *Energy Environ. Sci.*, 2014, **7**, 4104–4117.
27 S. M. Kim and S. I. Woo, *ChemSusChem*, 2012, **5**, 1513–1522.
28 S. Chaemchuen, N. A. Kabir, K. Zhou and F. Verpoort, *Chem. Soc. Rev.*, 2013, **42**, 9304–9332.
29 Y. Huang, Z. Lin, H. Fu, F. Wang, M. Shen, X. Wang and R. Cao, *ChemSusChem*, 2014, **7**, 2647–2653.
30 B. R. Pimentel, A. Parulkar, E. k. Zhou, N. A. Brunelli and R. P. Lively, *ChemSusChem*, 2014, **7**, 3202–3240.
31 S. Cavenati, C. A. Grande and A. E. Rodrigues, *Energy Fuels*, 2006, **20**, 2648–2659.
32 G. T. Rochelle, *Science*, 2009, 1652–1654.
33 Q. Yang, S. Vaesen, F. Ragon, A. D. Wiersum, D. Wu, A. Lago, T. Devic, C. Martineau, F. Taulelle and P. L. Llewellyn, *Angew. Chem.*, 2013, **125**, 10506–10510.
34 W. Lu, W. M. Verdegaal, J. Yu, P. B. Balbuena, H.-K. Jeong and H.-C. Zhou, *Energy Environ. Sci.*, 2013, **6**, 3559–3564.
35 S. Xiang, Y. He, Z. Zhang, H. Wu, W. Zhou, R. Krishna and B. Chen, *Nat. Commun.*, 2012, **3**, 954.
36 O. K. Farha, A. Ö. Yazaydın, I. Eryazici, C. D. Malliakas, B. G. Hauser, M. G. Kanatzidis, S. T. Nguyen, R. Q. Snurr and J. T. Hupp, *Nat. Chem.*, 2010, **2**, 944–948.
37 S. M. Kuznicki, V. A. Bell, S. Nair, H. W. Hillhouse, R. M. Jacubinas, C. M. Braunbarth, B. H. Toby and M. Tsapatsis, *Nature*, 2001, **412**, 720–724.
38 M. R. Hudson, W. L. Queen, J. A. Mason, D. W. Fickel, R. F. Lobo and C. M. Brown, *J. Am. Chem. Soc.*, 2012, **134**, 1970–1973.
39 A. D. K. Jones and T. Bekkedahl, *Nature*, 1997, **386**, 377.
40 P. Mohanty, L. D. Kull and K. Landskron, *Nat. Commun.*, 2011, **2**, 401.
41 S. Surblé, F. Millange, C. Serre, T. Düren, M. Latroche, S. Bourrelly, P. L. Llewellyn and G. Férey, *J. Am. Chem. Soc.*, 2006, **128**, 14889–14896.
42 Y. Xia, R. Mokaya, G. S. Walker and Y. Zhu, *Adv. Energy Mater.*, 2011, **1**, 678–683.

43 Y. Gong, H. Wang, Z. Wei, L. Xie and Y. Wang, *ACS Sustainable Chem. Eng.*, 2014, **2**, 2435–2441.
44 Y. Xue, B. Gao, Y. Yao, M. Inyang, M. Zhang, A. R. Zimmerman and K. S. Ro, *Chem. Eng. J.*, 2012, **200**, 673–680.
45 M. Sevilla, L. Yu, C. O. Ania and M. M. Titirici, *ChemElectroChem*, 2014, **1**, 2138–2145.
46 M.-M. Titirici, A. Thomas and M. Antonietti, *New J. Chem.*, 2007, **31**, 787–789.
47 M.-M. Titirici and M. Antonietti, *Chem. Soc. Rev.*, 2010, **39**, 103–116.
48 B. Hu, K. Wang, L. Wu, S. H. Yu, M. Antonietti and M. M. Titirici, *Adv. Mater.*, 2010, **22**, 813–828.
49 M. Sevilla, A. Fuertes and R. Mokaya, *Energy Environ. Sci.*, 2011, **4**, 1400–1410.
50 C. Falco, J. P. Marco-Lozar, D. Salinas-Torres, E. Morallón, D. Cazorla-Amorós, M.-M. Titirici and D. Lozano-Castelló, *Carbon*, 2013, **62**, 346–355.
51 M. Sevilla and A. B. Fuertes, *Energy Environ. Sci.*, 2011, **4**, 1765–1771.
52 M. Sevilla, C. Falco, M.-M. Titirici and A. B. Fuertes, *RSC Adv.*, 2012, **2**, 12792–12797.
53 M.-M. Titirici, *Sustainable Carbon Materials from Hydrothermal Processes*, Wiley Online Library, 2013.
54 M.-M. Titirici, R. J. White, C. Falco and M. Sevilla, *Energy Environ. Sci.*, 2012, **5**, 6796–6822.
55 M.-M. Titirici, R. J. White, N. Brun, V. L. Budarin, D. S. Su, F. del Monte, J. H. Clark and M. J. MacLachlan, *Chem. Soc. Rev.*, 2015, **44**, 250–290.
56 C. Falco, M. Sevilla, R. J. White, R. Rothe and M. M. Titirici, *ChemSusChem*, 2012, **5**, 1834–1840.
57 L. Yu, C. Falco, J. Weber, R. J. White, J. Y. Howe and M.-M. Titirici, *Langmuir*, 2012, **28**, 12373–12383.
58 M. Sevilla and A. B. Fuertes, *Chem.–Eur. J.*, 2009, **15**, 4195–4203.
59 M.-M. Titirici, M. Antonietti and N. Baccile, *Green Chem.*, 2008, **10**, 1204–1212.
60 N. K. Kang, B. Lee, S.-E. Shin, S. Jeon, M. S. Park and J.-W. Yang, *Bioresour. Technol.*, 2015, **181**, 231–237.
61 K. S. Sing, *Pure Appl. Chem.*, 1985, **57**, 603–619.
62 D. Qian, C. Lei, E. M. Wang, W. C. Li and A. H. Lu, *ChemSusChem*, 2014, **7**, 291–298.
63 J. Marco-Lozar, M. Kunowsky, F. Suárez-García, J. Carruthers and A. Linares-Solano, *Energy Environ. Sci.*, 2012, **5**, 9833–9842.
64 D. Cazorla-Amorós, J. Alcaniz-Monge and A. Linares-Solano, *Langmuir*, 1996, **12**, 2820–2824.
65 W. Xing, C. Liu, Z. Zhou, L. Zhang, J. Zhou, S. Zhuo, Z. Yan, H. Gao, G. Wang and S. Z. Qiao, *Energy Environ. Sci.*, 2012, **5**, 7323–7327.
66 Y. Zhao, L. Zhao, K. X. Yao, Y. Yang, Q. Zhang and Y. Han, *J. Mater. Chem.*, 2012, **22**, 19726–19731.
67 W. Shen and W. Fan, *J. Mater. Chem. A*, 2013, **1**, 999–1013.
68 G. P. Hao, W. C. Li, D. Qian and A. H. Lu, *Adv. Mater.*, 2010, **22**, 853–857.
69 W. Shen, Y. He, S. Zhang, J. Li and W. Fan, *ChemSusChem*, 2012, **5**, 1274–1279.
70 L. Liu, Q.-F. Deng, X.-X. Hou and Z.-Y. Yuan, *J. Mater. Chem.*, 2012, **22**, 15540–15548.
71 T. Chen, S. Deng, B. Wang, J. Huang, Y. Wang and G. Yu, *RSC Adv.*, 2015, **5**, 48323–48330.
72 M. C. Gutiérrez, D. Carriazo, C. O. Ania, J. B. Parra, M. L. Ferrer and F. del Monte, *Energy Environ. Sci.*, 2011, **4**, 3535–3544.
73 X. Zhu, P. C. Hillesheim, S. M. Mahurin, C. Wang, C. Tian, S. Brown, H. Luo, G. M. Veith, K. S. Han and E. W. Hagaman, *ChemSusChem*, 2012, **5**, 1912–1917.
74 Z. Zhang, J. Zhou, W. Xing, Q. Xue, Z. Yan, S. Zhuo and S. Z. Qiao, *Phys. Chem. Chem. Phys.*, 2013, **15**, 2523–2529.
75 B. Zhu, K. Li, J. Liu, H. Liu, C. Sun, C. E. Snape and Z. Guo, *J. Mater. Chem. A*, 2014, **2**, 5481–5489.
76 M. Sevilla, P. Valle-Vigón and A. B. Fuertes, *Adv. Funct. Mater.*, 2011, **21**, 2781–2787.
77 M. Yang, L. Guo, G. Hu, X. Hu, L. Xu, J. Chen, W. Dai and M. Fan, *Environ. Sci. Technol.*, 2015, **49**, 7063–7070.
78 X. Ma, Y. Li, M. Cao and C. Hu, *J. Mater. Chem. A*, 2014, **2**, 4819–4826.
79 G. Sethia and A. Sayari, *Carbon*, 2015, **93**, 68–80.
80 X. Fan, L. Zhang, G. Zhang, Z. Shu and J. Shi, *Carbon*, 2013, **61**, 423–430.
81 X. Ma, M. Cao and C. Hu, *J. Mater. Chem. A*, 2013, **1**, 913–918.
82 W. Lu, D. Yuan, J. Sculley, D. Zhao, R. Krishna and H.-C. Zhou, *J. Am. Chem. Soc.*, 2011, **133**, 18126–18129.
83 J. Song, W. Shen, J. Wang and W. Fan, *Carbon*, 2014, **69**, 255–263.
84 B. Ashourirad, A. K. Sekizkardes, S. Altarawneh and H. M. El-Kaderi, *Chem. Mater.*, 2015, **27**, 1349–1358.
85 Y. Sun and P. A. Webley, *Ind. Eng. Chem. Res.*, 2011, **50**, 9286–9294.
86 J.-R. Li, R. J. Kuppler and H.-C. Zhou, *Chem. Soc. Rev.*, 2009, **38**, 1477–1504.
87 S. Himeno, T. Komatsu and S. Fujita, *J. Chem. Eng. Data*, 2005, **50**, 369–376.
88 L. Wang and R. T. Yang, *J. Phys. Chem. C*, 2011, **116**, 1099–1106.
89 A. Wahby, J. M. Ramos-Fernández, M. Martínez-Escandell, A. Sepúlveda-Escribano, J. Silvestre-Albero and F. Rodríguez-Reinoso, *ChemSusChem*, 2010, **3**, 974–981.
90 M. Murialdo, N. P. Stadie, C. C. Ahn and B. Fultz, *J. Phys. Chem. C*, 2015, **119**, 944–950.
91 P.-Q. Liao, H. Chen, D.-D. Zhou, S.-Y. Liu, C.-T. He, Z. Rui, H. Ji, J.-P. Zhang and X.-M. Chen, *Energy Environ. Sci.*, 2015, **8**, 1011–1016.
92 J. Marco-Lozar, J. Juan-Juan, F. Suárez-García, D. Cazorla-Amorós and A. Linares-Solano, *Int. J. Hydrogen Energy*, 2012, **37**, 2370–2381.
93 J. Sim, H. Yim, N. Ko, S. B. Choi, Y. Oh, H. J. Park, S. Park and J. Kim, *Dalton Trans.*, 2014, **43**, 18017–18024.
94 M. E. Casco, M. Martínez-Escandell, E. Gadea-Ramos, K. Kaneko, J. Silvestre-Albero and F. Rodríguez-Reinoso, *Chem. Mater.*, 2015, **27**, 959–964.
95 D. Lozano-Castello, D. Cazorla-Amoros and A. Linares-Solano, *Energy Fuels*, 2002, **16**, 1321–1328.

96 M. Sevilla, R. Mokaya and A. B. Fuertes, *Energy Environ. Sci.*, 2011, **4**, 2930–2936.
97 Y. He, J.-H. Yun and N. A. Seaton, *Langmuir*, 2004, **20**, 6668–6678.
98 W. Zhu, J. Groen, A. Van Miltenburg, F. Kapteijn and J. Moulijn, *Carbon*, 2005, **43**, 1416–1423.
99 S. A. Al-Muhtaseb, F. A. Abu Al-Rub and M. Al Zarooni, *J. Chem. Eng. Data*, 2007, **52**, 60–65.
100 Z. Bao, S. Alnemrat, L. Yu, I. Vasiliev, Q. Ren, X. Lu and S. Deng, *Langmuir*, 2011, **27**, 13554–13562.
101 Y. He, R. Krishna and B. Chen, *Energy Environ. Sci.*, 2012, **5**, 9107–9120.
102 Y. Zhao, X. Liu, K. X. Yao, L. Zhao and Y. Han, *Chem. Mater.*, 2012, **24**, 4725–4734.
103 A. Myers and J. M. Prausnitz, *AIChE J.*, 1965, **11**, 121–127.
104 T. Ben, Y. Li, L. Zhu, D. Zhang, D. Cao, Z. Xiang, X. Yao and S. Qiu, *Energy Environ. Sci.*, 2012, **5**, 8370–8376.
105 Y. Shen and J. Bai, *Chem. Commun.*, 2010, **46**, 1308–1310.
106 J. Patiño, M. C. Gutiérrez, D. Carriazo, C. O. Ania, J. B. Parra, M. L. Ferrer and F. del Monte, *Environ. Sci. Technol.*, 2012, **5**, 8699–8707.
107 A. Aijaz, N. Fujiwara and Q. Xu, *J. Am. Chem. Soc.*, 2014, **136**, 6790–6793.
108 B. Yuan, X. Wu, Y. Chen, J. Huang, H. Luo and S. Deng, *Environ. Sci. Technol.*, 2013, **47**, 5474–5480.
109 J. Wang, R. Krishna, J. Yang and S. Deng, *Environ. Sci. Technol.*, 2015, **49**, 9364–9373.
110 Y. He, Z. Zhang, S. Xiang, H. Wu, F. R. Fronczek, W. Zhou, R. Krishna, M. O'Keeffe and B. Chen, *Chem.–Eur. J.*, 2012, **18**, 1901–1904.
111 D. Saha, Z. Bao, F. Jia and S. Deng, *Environ. Sci. Technol.*, 2010, **44**, 1820–1826.
112 N. Magnowski, A. Avila, C. Lin, M. Shi and S. Kuznicki, *Chem. Eng. Sci.*, 2011, **66**, 1697–1701.
113 Z. R. Herm, J. A. Swisher, B. Smit, R. Krishna and J. R. Long, *J. Am. Chem. Soc.*, 2011, **133**, 5664–5667.
114 J. Pires, V. K. Saini and M. L. Pinto, *Environ. Sci. Technol.*, 2008, **42**, 8727–8732.
115 V. K. Saini, M. Pinto and J. Pires, *Green Chem.*, 2011, **13**, 1251–1259.
116 Y. Belmabkhout and A. Sayari, *Chem. Eng. Sci.*, 2009, **64**, 3729–3735.
117 V. K. Saini, M. Andrade, M. L. Pinto, A. P. Carvalho and J. Pires, *Sep. Purif. Technol.*, 2010, **75**, 366–376.
118 G. S. Armatas and M. G. Kanatzidis, *Nat. Mater.*, 2009, **8**, 217–222.
119 A. P. Katsoulidis and M. G. Kanatzidis, *Chem. Mater.*, 2012, **24**, 471–479.